# **INORGANIC** CHEMISTRY







**FRONTIERS** 

## **RESEARCH ARTICLE**

View Article Online
View Journal | View Issue



**Cite this:** *Inorg. Chem. Front.*, 2025, **12**. 1881

# Three-dimensional porphyrin-based covalent organic frameworks as bifunctional electrocatalysts for oxygen reduction and evolution reactions†

Li Liao, ‡<sup>a,b</sup> Rui Wang, ‡<sup>c</sup> Zerong Zhang, <sup>c</sup> Jianfeng Zhang, <sup>c</sup> Shibin Huang, <sup>c</sup> Wenhao Xie, <sup>c</sup> Yiji Wang, <sup>c</sup> Ming Xue, <sup>b</sup> \*<sup>a</sup> Qianrong Fang <sup>b</sup> \*<sup>c</sup> and Shilun Qiu <sup>c</sup> \*<sup>c</sup>

The development of covalent organic frameworks (COFs) as bifunctional electrocatalysts for the oxygen reduction reaction (ORR) and the oxygen evolution reaction (OER), coupled with precise control over their active sites, is critical for advancing fuel cells and metal–air batteries. In this work, we present a series of three-dimensional (3D) COFs constructed from two strategically designed metal-porphyrin monomers. Among these, SUZ-101-Co stands out due to its high density of well-defined  $Co-N_4$  active sites, making it an outstanding bifunctional electrocatalyst. SUZ-101-Co exhibits an overpotential of only 240 mV at 10 mA cm<sup>-2</sup> for the OER and achieves a half-wave potential of 0.78 V for the ORR, showcasing its superior catalytic performance. Comprehensive experimental analyses and theoretical simulations attribute this remarkable activity to the abundance and accessibility of  $Co-N_4$  sites. This study not only underscores the potential of 3D COFs in electrocatalysis but also introduces a novel approach for designing energy conversion materials.

Received 26th November 2024, Accepted 18th January 2025 DOI: 10.1039/d4qi03018d

rsc.li/frontiers-inorganic

#### 10th anniversary statement

I am honored to congratulate *Inorganic Chemistry Frontiers* (ICF) on its 10th anniversary. I am Prof. Shilun Qiu from Jilin University, and since its launch in 2014, ICF has become a leading journal in inorganic and materials chemistry, providing a platform for global researchers to showcase innovative work. I have had the privilege of publishing in ICF since 2014, contributing regularly with an average of one paper per year. The journal has been instrumental in advancing my research in inorganic materials and continues to promote cutting-edge science in the field. I sincerely thank the editorial team, led by Prof. Song Gao, for their dedication and support. I look forward to ICF's continued success and its role in representing the forefront of inorganic chemistry.

#### Introduction

In recent years, metal-air batteries have drawn considerable attention as a promising energy conversion technology due to their high energy density and environmental advantages. <sup>1–5</sup> In these batteries, the oxygen evolution reaction (OER) and the

Covalent organic frameworks (COFs)<sup>21–28</sup> have become a hot material in the field of electrocatalysis in recent years due to their high specific surface area and well-defined crystal structure.<sup>29–32</sup> In particular, porphyrin-based COFs based on transition metal coordination are widely used in ORR/OER bifunctional electrocatalysts.<sup>33,34</sup> So far, most of the transition

10.1039/d4qi03018d

oxygen reduction reaction (ORR) are critical processes for charging and discharging, highlighting the need for cathode materials with high electrocatalytic activity for both reactions. Consequently, developing electrocatalysts that exhibit bifunctionality for the ORR and OER is of utmost importance. Although commercially available Pt/C-RuO<sub>2</sub> electrocatalysts have demonstrated excellent performance in the ORR and OER, their scarcity and environmental unfriendliness present significant challenges for large-scale deployment.

<sup>&</sup>lt;sup>a</sup>School of Chemical Engineering and Technology, School of Chemistry, GBRCE for Functional Molecular Engineering, IGCME, Sun Yat-sen University, Guangzhou, 510275, China. E-mail: xueming5@mail.sysu.edu.cn

bNortheast Guangdong Key Laboratory of New Functional Materials, School of Chemistry and Environment, Jiaying University, Meizhou, 514015, P.R. China State Key Laboratory of Inorganic Synthesis and Preparative Chemistry, Jilin University, Changchun 130012, P. R. China. E-mail: sqiu@jlu.edu.cn † Electronic supplementary information (ESI) available. See DOI: https://doi.org/

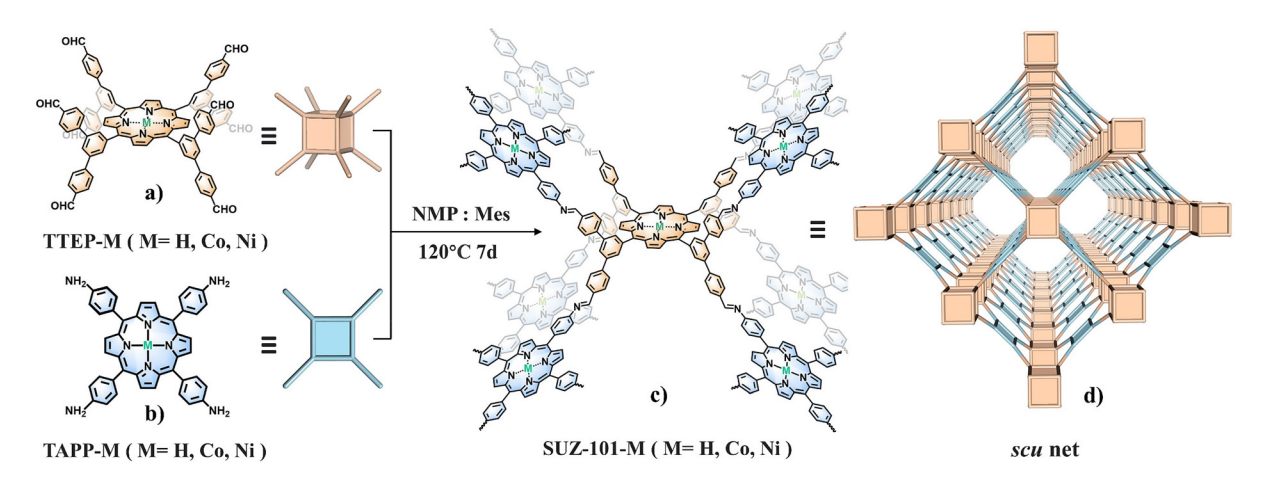
<sup>‡</sup>These authors contributed equally.

metal coordination porphyrins need to be pyrolyzed and then used as bifunctional electrocatalysts.35-37 However, the pyrolysis method wastes a lot of energy and brings structural uncertainty.<sup>38</sup> Therefore, it is of great significance to develop porphyrin-based COFs with transition metal coordination as ORR/ OER bifunctional electrocatalysts without pyrolysis. In recent years, only a handful of studies have reported similar results.<sup>39</sup> In 2022, Xu and Zeng's group reported two cobalt-coordinated porphyrin-based COFs containing diarylamine building blocks as ORR/OER bifunctional electrocatalysts. 40 It is worth noting that the Co-TAPP-PATA-COF synthesized by the group has a half-wave potential of 0.80 V during the ORR process and a potential of 420 mV at a current density of 10 mA cm<sup>-2</sup> when used as an OER electrocatalyst. In the same year, Tang et al. also reported a two-phase synthesis method of a hydrazidebased porphyrin COF film as a bifunctional electrocatalyst, which has a half-wave potential of 0.818 V in the alkaline electrolyte and a potential of 450 mV at a current density of 10 mA cm<sup>-2</sup> when used as an OER electrocatalyst. 41 Although these efforts have made remarkable progress, their performance in the OER is still far from that of advanced OER electrocatalysts.

Compared to 2D COFs, 3D COFs offer a higher specific surface area and a crystalline framework, enhancing mass transport and electron conduction for improved catalytic activity and stability. Their hierarchical porosity exposes more active sites (e.g., metal centers and porphyrin moieties), while their rigid, tunable architecture fosters synergistic interactions. Additionally, the integrated 3D architecture minimizes diffusion barriers, resulting in faster turnover and more efficient catalytic processes. Herein, we successfully produced a series of 3D COFs with high-density and well-structured frameworks, termed SUZ-101-M (where SUZ stands for SunYat-sen University Zhuhai and M represents H, Co, or Ni). Through the preloading of cobalt or nickel metal salts onto two pre-synthesized porphyrin-derived building blocks, we were able to create an ORR/OER bifunctional electrocatalyst

without the need for pyrolysis. Notably, the synthesized SUZ-101-Co displayed a half-wave potential of 0.78 V as an ORR electrocatalyst while functioning as an OER electrocatalyst with a low overpotential of just 240 mV at a current density of 10 mA cm<sup>-2</sup>. These findings strongly indicate the outstanding electrocatalytic performance of SUZ-101-Co. Theoretical simulations and coordination structure characterization further confirmed that the catalyst's high content of Co-N<sub>4</sub> sites is a critical factor contributing to its impressive catalytic activity. This study not only offers new insights for the design of efficient ORR/OER electrocatalysts but also underscores the remarkable potential of COF structures in the field of energy conversion.

Typically, SUZ-101-M was synthesized under conventional solvothermal conditions by polymerizing the 8-connected cubic-based building block, 5,10,15,20-tetrayl(tetrakis (([1,1':3',1"-terphenyl]-4,4"-dicarbaldehyde)))-porphyrin (TTEP) or its Co/Ni derivatives, with meso-tetrakis(4-aminophenyl)porphyrin (TAPP) or its Co/Ni derivatives (Scheme 1). A range of complementary characterization techniques was utilized to determine the structure. The formation of imine linkages was confirmed by the appearance of new peaks at approximately 1620 cm<sup>-1</sup> in the Fourier transform infrared (FT-IR) spectra. The successful conversion was additionally verified by the decrease of C=O and N-H vibrations at approximately 1701 cm<sup>-1</sup> and 3354 cm<sup>-1</sup>, respectively, in the FT-IR spectra (Fig. S8-S10†). Solid-state <sup>13</sup>C cross-polarization/magic-anglespinning (CP/MAS) NMR spectroscopy further confirmed the presence of imine groups, displaying a characteristic peak at around 160.30 ppm (Fig. S11†). Scanning electron microscopy (SEM) revealed that SUZ-101-M exhibited a rodlike morphology (Fig. S1-S3†), while transmission electron microscopy (TEM) indicated that the material consisted of microcrystalline aggregates (Fig. S4-S6†). TEM images did not show distinct nanoparticles for SUZ-101-Co and SUZ-101-Ni, suggesting that the metal was present as isolated sites. Energy-dispersive X-ray



Scheme 1 Molecular structures of (a) TTEP-M as an 8-connected cubic building block and (b) TAPP-M as a synergistic four-connected  $2D-D_{4h}$  monomer. (c) The expanded frameworks of 3D COFs, SUZ-101-M (M = H, Co, and Ni), synthesized through the condensation of TTEP-M and TAPP-M. (d) The scu topology representing the structural network of SUZ-101-M.

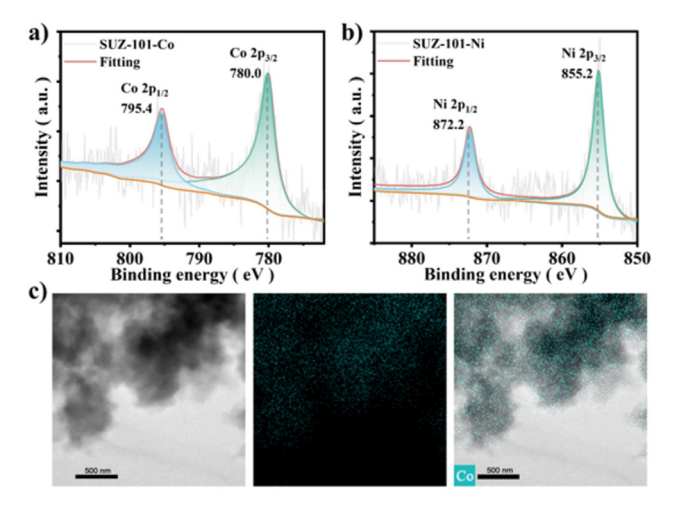


**Fig. 1** (a) High resolution Co 2p XPS profiles of SUZ-101-Co. (b) High resolution Ni 2p XPS profiles of SUZ-101-Ni. (c) EDX patterns corresponding to the elemental maps of SUZ-101-Co.

(EDX) mapping was employed to analyse the microcrystals of SUZ-101-Co and SUZ-101-Ni, confirming the uniform dispersion of metalloporphyrin sites throughout the framework (Fig. 1c and Fig. S7†). The metal content was found to be 5.67% for SUZ-101-Co and 5.13% for SUZ-101-Ni via inductively coupled plasma-optical emission (ICP-OES), which was consistent with the predicted values from the crystal structure analysis. The electronic states of the Co and Ni species were further investigated using X-ray photoelectron spectroscopy (XPS) (Fig. 1a, b and Fig. S16-S18†). Binding energies at approximately 780.0 and 795.4 eV for SUZ-101-Co and 855.2 and 872.2 eV for SUZ-101-Ni were attributed to the +2 oxidation states in the Co 2p and Ni 2p spectra, respectively. Thermogravimetric analysis (TGA) demonstrated that SUZ-101-M exhibited good thermal stability up to around 400 °C under a nitrogen atmosphere (Fig. S12†).

The crystalline structure of SUZ-101-M was verified by powder X-ray diffraction (PXRD) experiments combined with structural simulations using the Materials Studio software package. As shown in Fig. 2a, c, and e, each COF shows a series of sharp reflections, proving their crystalline nature. To further determine their lattice packing, the Materials Studio software package was used to construct the possible crystal model.<sup>43</sup> According to the reticular chemistry structure resource (RCSR),44 three nets including scu, sqc, and csq are reasonable for SUZ-101-M. All of these crystal models were then constructed and fully optimized by a density functional tight-binding (DFTB) method,45 as detailed in the ESI (Fig. S19-S21†). Among the three nets, the simulated PXRD pattern of the scu topology for SUZ-101-H, with cell parameters  $a = 52.2607 \text{ Å}, b = 13.0996 \text{ Å}, c = 52.2607 \text{ Å}, and <math>\alpha = \beta = \gamma = 90^{\circ}$ in the CMCM (no. 63) space group, closely matches the experimental results (Fig. 2a). SUZ-101-Co (a = 52.2186 Å, b =13.9009 Å, c = 52.2852 Å, and  $\alpha = \beta = \gamma = 90^{\circ}$ ) and SUZ-101-Ni  $(a = 51.2941 \text{ Å}, b = 13.8791 \text{ Å}, c = 52.2124 \text{ Å}, and } \alpha = \beta = \gamma = 90^{\circ})$ 

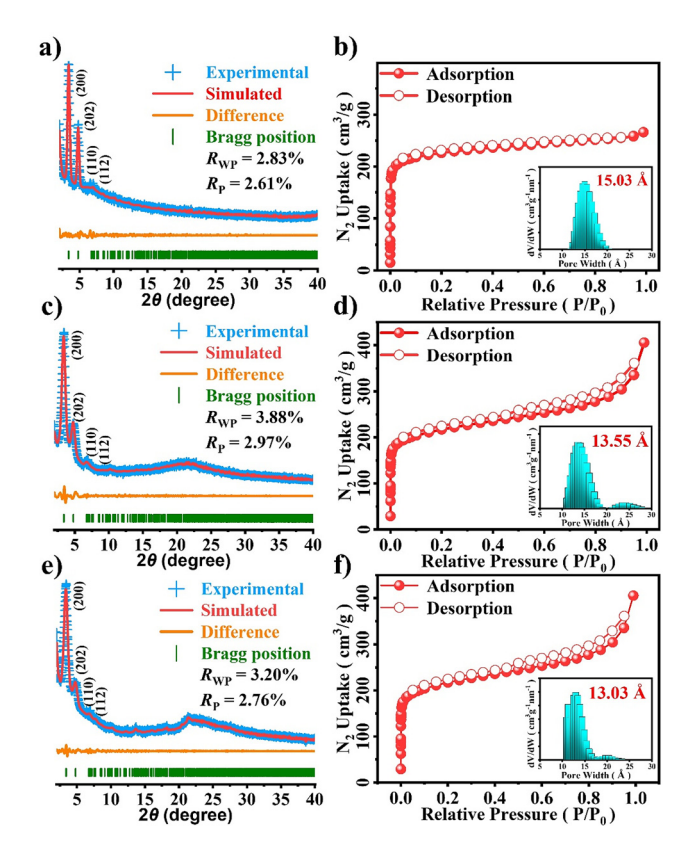


Fig. 2 Experimental and refined PXRD patterns of (a) SUZ-101-H, (c) SUZ-101-Co, and (e) SUZ-101-Ni.  $N_2$  adsorption—desorption isotherms of (b) SUZ-101-H, (d) SUZ-101-Co, and (f) SUZ-101-Ni at 77 K (inset: pore width profiles).

also share this space group (Fig. 2a, c and e). Furthermore, we carried out full profile pattern matching (Pawley) refinement. Peaks at 3.38°, 4.76°, 6.97°, and 7.73° correspond to the (200), (202), (110) and (112) facets of SUZ-101-H, those at 3.42°, 4.77°, 7.06°, and 7.71° correspond to the (200), (202), (110) and (112) facets of SUZ-101-Co, and those at 3.42°, 4.78°, 6.98°, and 7.74° correspond to the (200), (202), (110) and (112) facets of SUZ-101-Ni, respectively. The refinement results illustrated good agreement factors ( $R_P$  = 2.61% and  $R_{WP}$  = 2.83% were obtained for SUZ-101-H;  $R_P = 2.97\%$  and  $R_{WP} =$ 3.88% were obtained for SUZ-101-Co; and  $R_P = 2.76\%$  and  $R_{\rm WP}$  = 3.20% were obtained for SUZ-101-Ni). In contrast, for other possible structures, such as the sqc and csq nets, the calculated PXRD patterns are not in good agreement with the experimental ones (Fig. S22 and S23†). Based on the above results, the obtained SUZ-101-M samples are proposed to have the expected architectures with scu nets (Tables S2-S4†).

To further examine the pore structures of these crystalline frameworks, nitrogen adsorption–desorption isotherms were measured at 77 K. As shown in Fig. 2, all SUZ-101-M samples exhibited typical type I isotherms, which confirmed their microporous characteristics. The Brunauer–Emmett–Teller (BET) specific surface areas were 879 m<sup>2</sup> g<sup>-1</sup> for SUZ-101-H,

738 m² g⁻¹ for SUZ-101-Co and 716 m² g⁻¹ for SUZ-101-Ni (Fig. S13–S15†). Their pore-size distributions were calculated using nonlocal density functional theory (NLDFT), and each material showed a microporous pore width of 15.03 Å for SUZ-101-H, 13.55 Å for SUZ-101-Co and 13.03 Å for SUZ-101-Ni (Fig. 2b, d and f), aligning well with the modelled crystal structures (1.5 nm), thereby further verifying the  $\mathbf{scu}$  structure of SUZ-101-M.

For studying the catalytic activity of several COFs, we employed rotating ring-disk electrode (RRDE) measurements using linear sweep voltammetry (LSV) in a 0.1 M KOH solution to investigate the ORR performance of different catalysts. Due to the inherent low conductivity of COF materials, it is common to add certain conductive agents to enhance their conductivity.<sup>24</sup> Detailed methods for the preparation of COF-based catalyst inks are documented in the ESI.†

According to the recorded LSV curves, the SUZ-101-Co catalyst demonstrated the best electrocatalytic ORR activity among the series of catalysts studied, with an onset potential and half-wave potential of 0.84 V and 0.78 V, respectively, and a diffusion-limited current density reaching -5.6 mA cm<sup>-2</sup>. In comparison, SUZ-101-Ni exhibited an onset potential of 0.77 V, a half-wave potential of 0.66 V, and a diffusion-limited current density of -5.0 mA cm<sup>-2</sup>. The SUZ-101-H catalyst showed an onset potential of 0.72 V, a half-wave potential of 0.63 V, and a diffusion-limited current density of -3.4 mA cm<sup>-2</sup> at 0.2 V. The carbon black (CB) catalyst had onset and half-wave potentials of 0.69 V and 0.61 V, respectively, with a diffusionlimited current density of -2.7 mA cm<sup>-2</sup>. These results indicate that SUZ-101-Co exhibits significant advantages in ORR catalytic activity, providing a reference for further catalyst optimization. 46 Based on the results of the RRDE experiments, the calculations of the hydrogen peroxide yield and electron transfer number demonstrate that SUZ-101-Co exhibits a distinct four-electron transfer pathway within the voltage range of 0.2 to 0.7 V, with an electron transfer number ranging from 3.51 to 3.82 and a hydrogen peroxide yield between 9% and 24%. Similarly, SUZ-101-Ni also shows a four-electron transfer pathway in the same voltage range, with an electron transfer number ranging from 3.08 to 3.25 and a hydrogen peroxide yield reaching up to 37% to 46%. In contrast, the uncoordinated SUZ-101-H displays significantly lower electron transfer numbers, ranging from 2.4 to 2.7, but its hydrogen peroxide yield is considerably higher, between 65% and 81%, indicating a noticeable two-electron transfer pathway. These results suggest that metal coordination plays a crucial role in the electron transfer mechanism and product distribution, particularly in enhancing the efficiency of the four-electron transfer process.47

In addition to measuring the electrocatalytic performance of the ORR, the electrocatalytic performance of a series of COF-based electrocatalysts for the OER was measured. As shown in Fig. 3d, for SUZ-101-Co, the initial potential and overpotential at a current density of 10 mA cm<sup>-2</sup> were 1.42 V and 240 mV, respectively. For SUZ-101-Ni, the initial potential and overpotential at the same current density were 1.48 V and

310 mV. The initial potential and overpotential of SUZ-101-H without any metal coordination were significantly higher than those with coordinated metals, measuring 1.66 V and 560 mV at a current density of 10 mA cm $^{-2}$ , respectively. As for CB, the initial potential and overpotential at a current density of 10 mA cm $^{-2}$  were recorded at 1.78 V and 650 mV.

For ORR/OER electrocatalysts, the bifunctional potential  $(\Delta E)$  is a crucial parameter for evaluating their performance. It is typically defined as the difference between the OER potential at a current density of 10 mA cm<sup>-2</sup> and the half-wave potential of the ORR. As depicted in Fig. 3e, the E values for SUZ-101-H, SUZ-101-Co, SUZ-101-Ni, and CB are 1.16 V, 0.69 V, 0.88 V, and 1.27 V, respectively. It is worth noting that SUZ-101-Co exhibits the lowest  $\Delta E$  value among the synthesized electrocatalysts, which not only exceeds the performance of most COF-based bifunctional electrocatalysts reported in the existing literature but also outperforms other materials, such as carbon materials and transition metal materials (Table S1†).

The kinetic behaviours of a series of prepared catalysts in the ORR and OER were studied, with the Tafel slope used as an evaluation index. As shown in Fig. 3e and Fig. S24,† the Tafel slopes for the OER and ORR of SUZ-101-H are 294.85 mV dec<sup>-1</sup> and 52.92 mV dec<sup>-1</sup>, respectively; in contrast, the Tafel slopes of SUZ-101-Co significantly improved to 80.32 mV dec<sup>-1</sup> and 50.4 mV dec<sup>-1</sup>, indicating excellent reaction kinetics performance. Additionally, the Tafel slopes of nickel-coordinated SUZ-101-Ni for the OER and ORR are 76.03 mV dec<sup>-1</sup> and 87.52 mV dec<sup>-1</sup>, while the control group (CB) exhibits Tafel slopes of 298.74 mV dec<sup>-1</sup> and 69.91 mV dec<sup>-1</sup>. These results indicate that SUZ-101-Co demonstrates outstanding reaction kinetics characteristics in both OER and ORR processes compared to other catalysts.

Electrochemical impedance spectroscopy (EIS) was employed to examine the electronic transport behaviours of these porphyrin-based COF catalysts. The Nyquist plots revealed that the charge transfer resistances of SUZ-101-Co and SUZ-101-Ni were significantly lower than that of SUZ-101-H, indicating a substantial enhancement in the electron transfer capability of SUZ-101-H upon coordination with metal ions (Fig. 3g). To further elucidate the exceptional catalytic performance of the prepared catalysts, electrochemical double-layer capacitance  $(C_{dl})$  measurements were utilized to assess the electrochemically active surface area (ECSA) of several electrocatalysts (Fig. 3h and S24†). The calculated  $C_{\rm dl}$  values of SUZ-101-H, SUZ-101-Co, SUZ-101-Ni, and CB were 3.84 mF cm<sup>-2</sup>, 14.46 mF cm<sup>-2</sup>, 7.78 mF cm<sup>-2</sup>, and 2.33 mF cm<sup>-2</sup>, respectively. These data indicate that SUZ-101-Co exposes a greater number of active sites during the ORR and OER, showcasing superior catalytic activity compared to the other synthesized electrocatalysts. The improvement in electronic transport characteristics, coupled with the increase in electrochemically active surface area, strongly supports the outstanding catalytic performance of SUZ-101-Co, thereby confirming the beneficial role of metal incorporation in optimizing the catalyst efficiency.

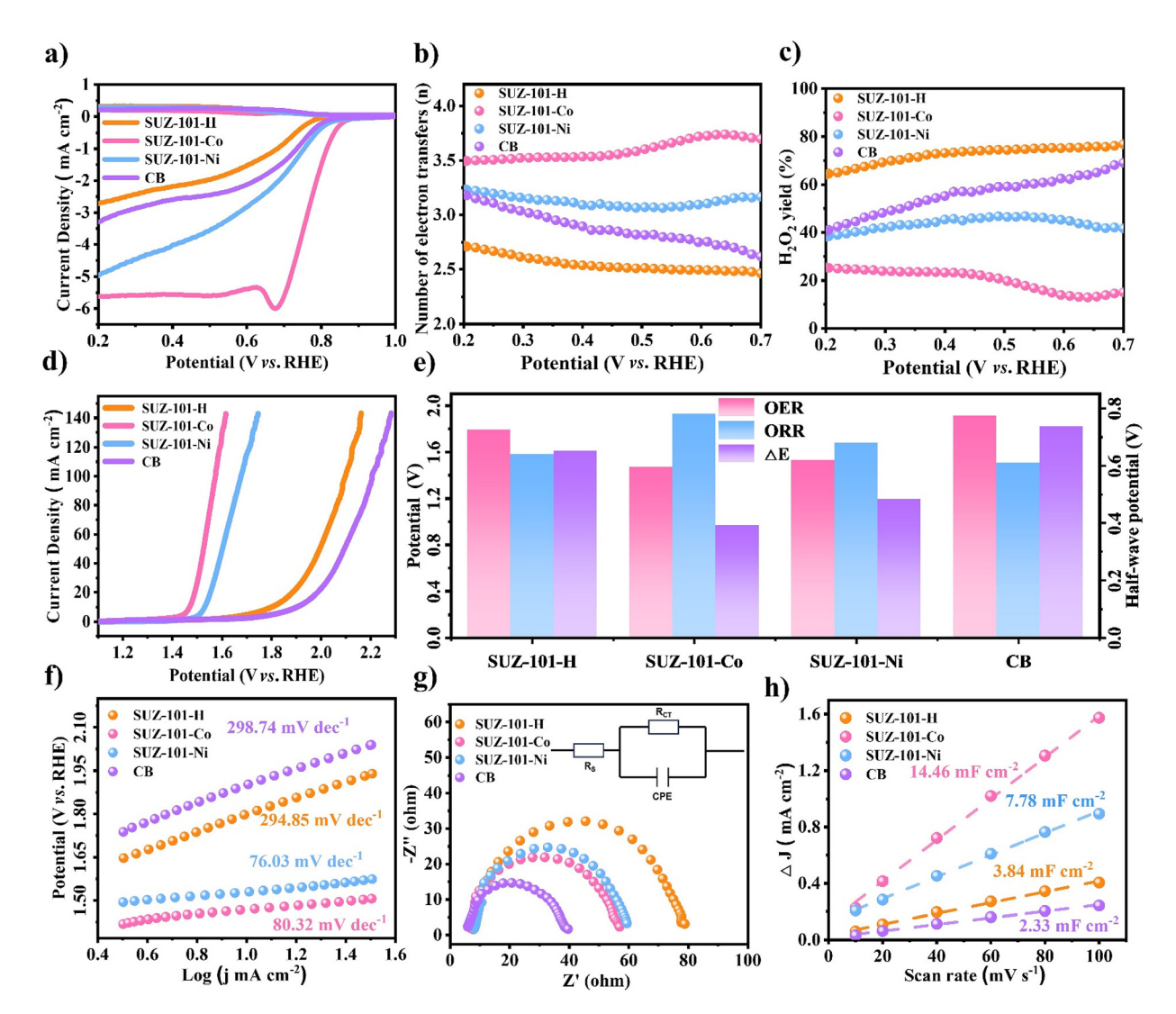


Fig. 3 (a) LSV curves of SUZ-101-H, SUZ-101-Co, SUZ-101-Ni and CB in an O2-saturated 0.1 M KOH electrolyte for the ORR. (b) The electron transfer number and (c) the corresponding H<sub>2</sub>O<sub>2</sub> selectivity of SUZ-101-H (orange), SUZ-101-Co (pink), SUZ-101-Ni (blue) and CB (purple) calculated from the RRDE results in O2-saturated 0.1 M KOH. (d) LSV curves of SUZ-101-H, SUZ-101-Co, SUZ-101-Ni and CB in an O2-saturated 0.1 M KOH electrolyte for the OER. (e) The half-wave potential of the ORR catalyst calculated from the LSV curve and the overpotential at a current density of 10 mA cm<sup>-2</sup> and the difference between them. (f) The corresponding Tafel slopes of SUZ-101-H (orange), SUZ-101-Co (pink), SUZ-101-Ni (blue) and CB (purple) in O<sub>2</sub>-saturated 0.1 M KOH for the OER. (g) Impedance measurements for SUZ-101-H (orange), SUZ-101-Co (pink), SUZ-101-Ni (blue) and CB (purple). Inset: the equivalent electric circuit. (h) C<sub>dl</sub> measurements of SUZ-101-H (orange), SUZ-101-Co (pink), SUZ-101-Ni (blue) and CB (purple) in O2-saturated 0.1 M KOH.

Stability is a crucial indicator for assessing catalyst performance.<sup>50</sup> To evaluate the excellent catalytic performance of SUZ-101-Co, we conducted long-term durability tests using chronopotentiometry. As illustrated in Fig. S26,† SUZ-101-Co maintains long-term stability for approximately 20 hours at an applied current density of 10 mA cm<sup>-2</sup> during the OER. Furthermore, in the case of the ORR, its half-wave current density demonstrates remarkable durability over the same period of 20 hours. We also measured the effectiveness of SUZ-101-Co and commercial RuO2 catalysts at 1.5 V vs. the current density at the voltage of the RHE changes over time. As shown in Fig. S26,† the OER performance of the synthesized SUZ-101-Co is basically not degraded within 20 hours. When

used as an ORR catalyst, it has good stability at the same voltage compared to commercial Pt/C catalysts within 20 hours. Additionally, we examined the anti-poisoning effect of SUZ-101-Co in the presence of methanol. As shown in Fig. S27,† the experiment revealed that following the addition of methanol, the current density quickly recovered to its initial state within 100 seconds. These findings indicate that SUZ-101-Co exhibits excellent long-term stability and effective anti-poisoning capability.

To conduct an in-depth study of the catalytic activity of SUZ-101-Co, the primary focus lies in exploring its coordination mode. A comparison of the Co K-edge XANES spectra between SUZ-101-Co and the Co porphyrin monomer (Pro-Co)

reveals a notable similarity in their curves, indicating that the atomic environments of cobalt in both cases are essentially identical (Fig. 4a). A closer examination of the Fourier-transform EXAFS curves for SUZ-101-Co and Pro-Co (Fig. 4b) shows that both exhibit a pronounced signal at 1.53 Å, corresponding to Co-N scattering pathways.<sup>51</sup> This finding suggests that there is no significant change in the cobalt coordination environment before and after coordination. Co-N interactions can be clearly identified, indicating that a single cobalt atom coordinates with N atoms to form a typical Co-N-C active site.<sup>52</sup> In addition, the cobalt element exhibits an oxidation state slightly below +2, as detected by the cobalt 2p XPS spectra (Fig. S17†) and the cobalt L edge XANES spectra (Fig. 4), which is consistent with the structure of a typical Co-N-C single-atom site.<sup>53</sup> The above results unambiguously characterize Co-N-C catalysts as a single-atom catalyst (SAC) with atomically dispersed Co-N-C sites, thus confirming that the click-limit strategy is an efficient synthetic method for the preparation of M-N-C SAC.54 To gain a clearer understanding of the structure of SUZ-101-Co, the EXAFS data are fitted using a Co-N<sub>4</sub> coordination model.<sup>55</sup> The results indicate that the cobalt sites in both SUZ-101-Co and Pro-Co are coordinated with four nitrogen atoms (Fig. 4c). These experimental findings suggest that the catalytic activity of SUZ-101-Co is likely closely linked to its stable Co-N<sub>4</sub> coordination environment.

To explore the differences in the ORR and OER activities between SUZ-101-Co and SUZ-101-Ni, density functional theory (DFT) calculations were conducted to analyse the free energy of both catalysts during the ORR and OER processes. The results, based on the optimized configurations of the COF

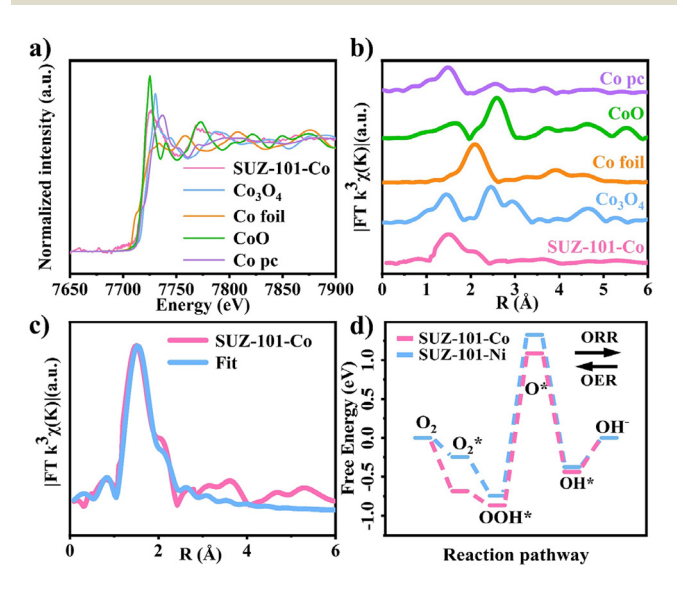


Fig. 4 (a) Normalized Co K-edge XANES spectra of SUZ-101-Co (pink), Co<sub>3</sub>O<sub>4</sub> (blue), Co-foil (orange), CoO (green) and Co pc (purple). (b) Co space in the K-edge Fourier transform EXAFS spectra of SUZ-101-Co (pink), Co<sub>3</sub>O<sub>4</sub> (blue), Co-foil (orange), CoO (green) and Co pc (purple). (c) EXAFS fitting curves of SUZ-101-Co. (d) The calculated free energy diagrams of SUZ-101-Co and SUZ-101-Ni for catalysing the ORR and OER.

molecular fragments, are illustrated in Fig. S28.† The study reveals that for both the ORR and OER, the rate-determining step for both catalysts involves the formation of O\* from OOH\* (Fig. 4d). Further analysis indicates that the free energy change  $(\Delta G)$  of SUZ-101-Co is 1.942 eV, while that of SUZ-101-Ni is 2.068 eV. This suggests that SUZ-101-Co exhibits higher catalytic activity during the ORR and OER processes, which aligns with experimental observations.<sup>56</sup> Additionally, solid-state UVvisible diffuse reflectance spectroscopy was employed to calculate the band gaps of SUZ-101-H, SUZ-101-Co, and SUZ-101-Ni. As demonstrated in Fig. S29-S31,† the band gaps of SUZ-101-H, SUZ-101-Co, and SUZ-101-Ni are 2.87 eV, 2.52 eV, and 2.56 eV, respectively. Notably, SUZ-101-Co has the smallest band gap, a critical factor contributing to its superior electrocatalytic activity. These findings not only provide a quantitative comparison of the performance of different catalysts but also offer a theoretical foundation for subsequent catalyst design and optimization.57

# Conclusions

In summary, we synthesized a series of 3D COFs with high metal loading by pre-loading the porphyrin monomers. Among them, SUZ-101-Co exhibits excellent catalytic performance as an electrocatalytic ORR/OER bifunctional catalyst. As an ORR electrocatalyst, it has a half-wave potential of up to 0.78 V, and as an OER electrocatalyst, its overpotential is only 240 mV at a current density of 10 mA cm $^{-2}$ . To the best of our knowledge, this result is not only superior to the vast majority of ORR/OER bifunctional electrocatalysts reported so far but also represents the first example of 3D COFs as ORR/OER bifunctional electrocatalysts. This work provides new insights for the development of ORR/OER bifunctional COF-based electrocatalysts in energy storage and conversion systems.

#### Author contributions

Li Liao and Rui Wang: investigation, conceptualization, methodology, data curation, and writing - original draft. Zerong Zhang, Jianfeng Zhang, Shibin Huang, Wenhao Xie and Yiji Wang: methodology, software, supervision, validation, and writing - review and editing. Shilun Qiu, Ming Xue, and Qianrong Fang: methodology, funding acquisition, software, and supervision.

# Data availability

The data supporting this article have been included as part of the ESI.†

#### Conflicts of interest

There are no conflicts to declare.

# Acknowledgements

This work was supported by the National Key R&D Program of China (2022YFB3704900 and 2021YFF0500500), the National Natural Science Foundation of China (22025504, 21621001, and 22105082), the SINOPEC Research Institute of Petroleum Processing, the "111" Project (BP0719036 and B17020), and the China Postdoctoral Science Foundation (2020TQ0118 and 2020M681034).

#### References

- 1 X. Chi, M. Li, J. Di, P. Bai, L. Song, X. Wang, F. Li, S. Liang, J. Xu and J. Yu, A highly stable and flexible zeolite electrolyte solid-state Li-air battery, *Nature*, 2021, **592**, 551–557.
- 2 B. Ge, L. Hu, X. Yu, L. Wang, C. Fernandez, N. Yang, Q. Liang and Q. H. Yang, Engineering Triple-Phase Interfaces around the Anode toward Practical Alkali Metal-Air Batteries, *Adv. Mater.*, 2024, 36, 2400937.
- 3 Y. Li, A. Huang, L. Zhou, B. Li, M. Zheng, Z. Zhuang, C. Chen, C. Chen, F. Kang and R. Lv, Main-group element-boosted oxygen electrocatalysis of Cu-N-C sites for zinc-air battery with cycling over 5000 h, *Nat. Commun.*, 2024, 15, 8365–8365.
- 4 T. Zhou, H. Shan, H. Yu, C. a. Zhong, J. Ge, N. Zhang, W. Chu, W. Yan, Q. Xu, H. a. Wu, C. Wu and Y. Xie, Nanopore Confinement of Electrocatalysts Optimizing Triple Transport for an Ultrahigh-Power-Density Zinc-Air Fuel Cell with Robust Stability, *Adv. Mater.*, 2020, 32, 2003251.
- 5 J. Park, C. Lee, J. Ju, J. Lee, J. Seol, S. Lee and J. Kim, Bifunctional Covalent Organic Framework-Derived Electrocatalysts with Modulated p-Band Centers for Rechargeable Zn–Air Batteries, *Adv. Funct. Mater.*, 2021, 31, 2101727.
- 6 R. Wang, Z. Zhang, J. Suo, L. Liao, L. Li, Z. Yu, H. Zhang, V. Valtchev, S. Qiu and Q. Fang, Exploring metal-free ionic covalent organic framework nanosheets as efficient OER electrocatalysts via cationic-π interactions, *Chem. Eng. J.*, 2023, 478, 147403.
- 7 H. Li, G. Yan, H. Zhao, P. C. Howlett, X. Wang and J. Fang, Earthworm-Inspired Co/Co<sub>3</sub>O<sub>4</sub>/CoF<sub>2</sub>@NSC Nanofibrous Electrocatalyst with Confined Channels for Enhanced ORR/ OER Performance, *Adv. Mater.*, 2024, 36, 2311272.
- 8 S. Ji, Y. Mou, H. Liu, X. Lu, Y. Zhang, C. Guo, K. Sun, D. Liu, J. H. Horton, C. Wang, Y. Wang and Z. Li, Manipulating the Electronic Properties of an Fe Single Atom Catalyst via Secondary Coordination Sphere Engineering to Provide Enhanced Oxygen Electrocatalytic Activity in Zinc-Air Batteries, Adv. Mater., 2024, 36, 2410121.
- 9 L. Huo, M. Lv, M. Li, X. Ni, J. Guan, J. Liu, S. Mei, Y. Yang, M. Zhu, Q. Feng, P. Geng, J. Hou, N. Huang, W. Liu, X. Y. Kong, Y. Zheng and L. Ye, Amorphous MnO<sub>2</sub> Lamellae Encapsulated Covalent Triazine Polymer-Derived Multi-

- Heteroatoms-Doped Carbon for ORR/OER Bifunctional Electrocatalysis, *Adv. Mater.*, 2024, **36**, 2312868.
- 10 X. Xu, S. Zhang, K. Xu, H. Chen, X. Fan and N. Huang, Janus Dione-Based Conjugated Covalent Organic Frameworks with High Conductivity as Superior Cathode Materials, J. Am. Chem. Soc., 2023, 145, 1022–1030.
- 11 W. Li, J. Wang, J. Chen, K. Chen, Z. Wen and A. Huang, Core-Shell Carbon-Based Bifunctional Electrocatalysts Derived from COF@MOF Hybrid for Advanced Rechargeable Zn-Air Batteries, Small, 2022, 18, 2202018.
- 12 X. Zhong, X. Xiao, Q. Li, M. Zhang, Z. Li, L. Gao, B. Chen, Z. Zheng, Q. Fu, X. Wang, G. Zhou and B. Xu, Understanding the active site in chameleon-like bifunctional catalyst for practical rechargeable zinc-air batteries, *Nat. Commun.*, 2024, 15, 9616–9616.
- 13 C. Zhao, J. Liu, J. Wang, D. Ren, B. Li and Q. Zhang, Recent advances of noble-metal-free bifunctional oxygen reduction and evolution electrocatalysts, *Chem. Soc. Rev.*, 2021, 50, 7745–7778.
- 14 G. Chen, Y. Liu, S. Xue, R. Zhang, H. Lv, J. Zhang, L. Wu and R. Che, Exceptionally Bifunctional ORR/OER Performance via Synergistic Atom-Cluster Interaction, Small, 2024, 20, 2308192.
- 15 M. A. Alkhalifah, B. Howchen, J. Staddon, V. Celorrio, D. Tiwari and D. J. Fermin, Correlating Orbital Composition and Activity of LaMn<sub>x</sub>Ni<sub>1-x</sub>O<sub>3</sub> Nanostructures toward Oxygen Electrocatalysis, *J. Am. Chem. Soc.*, 2022, 144, 4439–4447.
- 16 C. Zhou, X. Chen, S. Liu, Y. Han, H. Meng, Q. Jiang, S. Zhao, F. Wei, J. Sun, T. Tan and R. Zhang, Super durable Bifunctional Oxygen Electrocatalyst for High-Performance Zinc-Air Batteries, J. Am. Chem. Soc., 2022, 144, 2694–2704.
- 17 Y. Liu, Z. Chen, Z. Li, N. Zhao, Y. Xie, Y. Du, J. Xuan, D. Xiong, J. Zhou, L. Cai and Y. Yang, CoNi nanoalloy-Co-N<sub>4</sub> composite active sites embedded in hierarchical porous carbon as bi-functional catalysts for flexible Zn-air battery, *Nano Energy*, 2022, 99, 107325.
- 18 B. Wei, Z. Fu, D. Legut, T. C. Germann, S. Du, H. Zhang, J. S. Francisco and R. Zhang, Rational Design of Highly Stable and Active MXene-Based Bifunctional ORR/OER Double-Atom Catalysts, Adv. Mater., 2021, 33, 2102595.
- 19 H. Li, W. Wang, S. Xue, J. He, C. Liu, G. Gao, S. Di, S. Wang, J. Wang, Z. Yu and L. Li, Superstructure-Assisted Single-Atom Catalysis on Tungsten Carbides for Bifunctional Oxygen Reactions, J. Am. Chem. Soc., 2024, 146, 9124–9133.
- 20 M. Wang, C. Wang, J. Liu, F. Rong, L. He, Y. Lou, Z. Zhang and M. Du, Efficient Ag/Ag<sub>2</sub>O-Doped Cobalt Metallo-Covalent Organic Framework Electrocatalysts for Rechargeable Zinc-Air Battery, ACS Sustainable Chem. Eng., 2021, 9, 5872–5883.
- 21 P. Adrien, I. Annabelle, W. Nathan, O. Michael, J. Adam and M. Omar, Porous, Crystalline, Covalent Organic Frameworks, *Science*, 2005, **310**, 1166–1170.
- 22 C. S. Diercks and O. M. Yaghi, The atom, the molecule, and the covalent organic framework, *Science*, 2017, 355, eaal1585.

23 X. Guan, Q. Fang, Y. Yan and S. Qiu, Functional Regulation and Stability Engineering of Three-Dimensional Covalent Organic Frameworks, Acc. Chem. Res., 2022, 55, 1912-1927.

Research Article

- 24 X. Feng, X. Ding and D. Jiang, Covalent organic frameworks, Chem. Soc. Rev., 2012, 41, 6010-6022.
- 25 L. Liao, Z. Zhang, X. Guan, H. Li, Y. Liu, M. Zhang, B. Tang, V. Valtchev, Y. Yan, S. Qiu, X. Yao and Q. Fang, Three-Dimensional sp<sup>2</sup> Carbon-Linked Covalent Organic Frameworks as a Drug Carrier Combined with Fluorescence Imaging, Chin. J. Chem., 2022, 40, 2081-2088.
- 26 L. Liao, X. Guan, H. Zheng, Z. Zhang, Y. Liu, H. Li, L. Zhu, S. Qiu, X. Yao and Q. Fang, Three-dimensional microporous and mesoporous covalent organic frameworks based on cubic building units, Chem. Sci., 2022, 32, 9305-
- 27 Y. Liu, J. Ren, Y. Wang, X. Zhu, X. Guan, Z. Wang, Y. Zhou, L. Zhu, S. Qiu, S. Xiao and Q. Fang, A Stable Luminescent Covalent Organic Framework Nanosheet for Sensitive Molecular Recognition, CCS Chem., 2023, 5, 2033-2045.
- 28 Z. Wang, Y. Liu, Y. Wang and Q. Fang, A New Covalent Organic Framework Modified with Sulfonic Acid for CO2 Uptake and Selective Dye Adsorption, Acta Chim. Sin., 2022, 80, 37-43.
- 29 X. Guan, F. Chen, S. Qiu and Q. Fang, Three-Dimensional Covalent Organic Frameworks: From Synthesis to Applications, Angew. Chem., Int. Ed., 2023, 62, e202213203.
- 30 J. Wang, W. Li, Y. Li and A. Huang, Space-Confined Growth of Co9S8 Nanoparticles in Covalent Organic Framework-Derived Porous Carbon for Efficient Bifunctional Oxygen Electrocatalysis, Adv. Sustainable Syst., 2024, 8, 2300301.
- 31 Z. Shan, Y. Sun, M. Wu, Y. Zhou, J. Wang, S. Chen, R. Wang and G. Zhang, Metal-porphyrin-based three-dimensional covalent organic frameworks for electrocatalytic nitrogen reduction, Appl. Catal., B, 2024, 342, 123418.
- 32 P. Jhariat, A. Warrier, A. Sasmal, S. Das, S. Sarfudeen, P. Kumari, A. K. Nayak and T. Panda, Reticular synthesis of two-dimensional ionic covalent organic networks as metalfree bifunctional electrocatalysts for oxygen reduction and evolution reactions, Nanoscale, 2024, 16, 5665-5673.
- 33 S. Huang, K. Chen and T. Li, Porphyrin and phthalocyanine based covalent organic frameworks for electrocatalysis, Coord. Chem. Rev., 2022, 464, 214563.
- 34 J. Gu, Y. Peng, T. Zhou, J. Ma, H. Pang and Y. Yamauchi, Porphyrin-based framework materials for energy conversion, Nano Res. Energy, 2022, 1, 9120009.
- 35 B. Li, C. Zhao, S. Chen, J. Liu, X. Chen, L. Song and Q. Zhang, Framework-Porphyrin-Derived Single-Atom Bifunctional Oxygen Electrocatalysts and their Applications in Zn-Air Batteries, Adv. Mater., 2019, 31, 1900592.
- 36 S. Ren, J. Wang and X. Xia, Highly Efficient Oxygen Reduction Electrocatalyst Derived from a New Three-Dimensional PolyPorphyrin, ACS Appl. Mater. Interfaces, 2016, 8, 25875.
- 37 Y. Mo, S. Liu, G. Liu, G. Wang and W. Lu, Bimetal Covalent Organic Frameworks/Carbon Nanotube-Derived Iron-, Cobalt- and Nitrogen-Codoped Catalysts for Efficient

- Oxygen Electrocatalysis and Zinc-Air Batteries, ChemNanoMat, 2022, 8, e202200330.
- 38 X. Cui, L. Gao, R. Ma, Z. Wei, C. Lu, Z. Li and Y. Yang, Pyrolysis-free covalent organic framework-based materials for efficient oxygen electrocatalysis, J. Mater. Chem. A, 2021, 9, 20985.
- 39 J. Li, Y. Tan, J. Lin, Y. Feng, X. Zhang, E. Zhou, D. Yuan and Y. Wang, Coupling electrocatalytic redox-active sites in a three-dimensional bimetalloporphyrin-based organic framework for enhancing carbon dioxide reduction and oxygen evolution, J. Mater. Chem. A, 2024, 12, 9478-9485.
- 40 M. Liu, S. Liu, C. Cui, Q. Miao, Y. He, X. Li, Q. Xu and G. Zeng, Construction of Catalytic Covalent Organic Frameworks with Redox-Active Sites for the Oxygen Reduction and the Oxygen Evolution Reaction, Angew. Chem., 2022, 134, e202213522.
- 41 J. Tang, Z. Liang, H. Qin, X. Liu, B. Zhai, Z. Su, Q. Liu, H. Lei, K. Liu, C. Zhao, R. Cao and Y. Fang, Large-area Free-standing Metalloporphyrin-based Covalent Organic Framework Films by Liquid-air Interfacial Polymerization for Oxygen Electrocatalysis, Angew. Chem., 2023, 135, e202214449.
- 42 R. Wang, J. Zhao, Q. Fang and S. Qiu, Advancements and applications of three-dimensional covalent organic frameworks, Chem. Synth., 2024, 4, 29.
- 43 Materials Studio, ver. 7.0, Accelrys Inc, San Diego, CA.
- 44 M. O'Keeffe, M. A. Peskov, S. J. Ramsden and O. M. Yaghi, Acc. Chem. Res., 2008, 41, 1782-1789.
- 45 F. Spiegelman, N. Tarrat, J. Cuny, L. Dontot, E. Posenitskiy, C. Martí and C. Rapacioli, Density-functional tightbinding: basic concepts and applications to molecules and clusters, Adv. Phys.: X, 2020, 5, 1710252.
- 46 D. Wu, Q. Xu, J. Qian, X. Li and Y. Sun, Bimetallic Covalent Organic Frameworks for Constructing Multifunctional Electrocatalyst, Chem. - Eur. J., 2019, 25, 3105.
- 47 R. Wang, Z. Zhang, H. Zhou, M. Yu, L. Liao, Y. Wang, S. Wan, H. Lu, W. Xing, V. Valtchev, S. Qiu and Q. Fang, Structural Modulation of Covalent Organic Frameworks for Efficient Hydrogen Peroxide Electrocatalysis, Angew. Chem., Int. Ed., 2024, 63, e202410417.
- 48 H. Zong, W. Liu, M. Li, S. Gong, K. Yu and Z. Zhu, Oxygen-T erminated Nb<sub>2</sub>CO<sub>2</sub> MXene with Interfacial Self-Assembled COF as a Bifunctional Catalyst for Durable Zinc-Air Batteries, ACS Appl. Mater. Interfaces, 2022, 14, 10738.
- 49 R. Wang, H. Zhou, Q. Pan, Z. Su, S. Qiu, Q. Fang and H. Lu, Ionic covalent organic framework-MXene heterojunction constructed by electrostatic interaction for stable electrocatalytic hydrogen generation, Chem. Eng. J., 2024, 499, 156033.
- 50 F. Pei, M. Chen, F. Kong, Y. Huang and X. Cui, In situ coupling FeN nanocrystals with Fe/Fe<sub>3</sub>C nanoparticles to N-doped carbon nanosheets for efficient oxygen electrocatalysis, Appl. Surf. Sci., 2022, 587, 152922.
- 51 S. Chi, Q. Chen, S. Zhao, D. Si, Q. Wu, Y. Huang and R. Cao, Three-dimensional porphyrinic covalent organic

- frameworks for highly efficient electroreduction of carbon dioxide, J. Mater. Chem. A, 2022, 10, 4653.
- 52 C. Zhao, J. Liu, J. Wang, C. Wang, X. Guo, X. Li, X. Chen, L. Song, B. Li and Q. Zhang, A clicking confinement strategy to fabricatetransition metal single-atom sites for bifunctionaloxygen electrocatalysis, Sci. Adv., 2022, 8, eabn5091.
- 53 H. Zhou, K. Li, Q. Pan, Z. Su and R. Wang, Application of nanocomposites in covalent organic framework-based electrocatalysts, Nanomaterials, 2024, 14, 1907.
- 54 W. Liu, L. Zhang, W. Yan, X. Liu, X. Yang, S. Miao, W. Wang, A. Wang and T. Zhang, Single-atomdispersed Co-N-C catalyst: Structure identification and performance for hydrogenative coupling of nitroarenes, Chem. Sci., 2016, 7, 5758-5764.
- 55 L. Gong, B. Chen, Y. Gao, B. Yu, Y. Wang, B. Han, C. Lin, Y. Bian, D. Qi and J. Jiang, Covalent organic frameworks based on tetraphenyl-p-phenylenediamine and metalloporphyrin for electrochemical conversion of CO2 to CO, Inorg. Chem. Front., 2022, 9, 3217.
- 56 Z. Chen, H. Zheng, J. Zhang, Z. Jiang, C. Bao, C. Yeh and N. Lai, Covalent organic frameworks derived Single-Atom cobalt catalysts for boosting oxygen reduction reaction in rechargeable Zn-Air batteries, J. Colloid Interface Sci., 2024, 670, 103.
- 57 X. Zhang, Z. Lin, W. Su, M. Zhang, X. Wang and K. Li, High-efficiency power amplification of microbial fuel cell by modifying cathode with iron-incorporated thermalized covalent organic framework, Appl. Surf. Sci., 2022, 592, 153278.